X-Radiation in Health and Disease: Novel Approaches to the Study of Disease Processes and Therapy

D.E. Myers[a,b,c], A.W. Stevenson[d,e], S.W. Wilkins[d], T.J. O'Brien[f], R.J. Hicks[g], S.C. Mayo[d], A. Maksimenko[e], G.F. Moorhead[d], C.G. Ryan[h], S. James[i], M.L. Broadhead[j], D. Patterson[e], M.D de Jonge[e], D. Howard[e], D. Häusermann[e]

[a] *College of Health and Biomedicine, Victoria University, Australia*
[b] *Departments of Medicine, Western and Eastern Precincts, University of Melbourne*
[c] *Australian Institute for Musculoskeletal Science, Victoria University and University of Melbourne*
[d] *Materials Science and Engineering, CSIRO, Clayton, Australia*
[e] *Australian Synchrotron, Clayton, Australia*
[f] *Department of Medicine, Royal Melbourne Hospital, University of Melbourne, Australia*
[g] *Peter MacCallum Cancer Centre, University of Melbourne, Australia*
[h] *Earth Science and Resource Engineering, CSIRO, Clayton, Australia*
[i] *Florey Department of Neuroscience and Mental Health, Parkville, Australia*
[j] *School of Medicine and Public Health, University of Newcastle, Australia*

The purpose of this overview is to relate some biomedical and clinical applications from the Australian Synchrotron that highlight how it benefits the Australian medical research community. The Australian Synchrotron (AS) was proposed by the Australian Academy of Science in 1989 and was finally approved in 2001 with the main building being established over a period of 5 years. Beam lines were being activated progressively from that time through to the end of the decade. The first beamline to collect data was the MX1 beamline and the last, as well as the most ambitious and most complex, was the Imaging and Medical Therapy (IMT) Beamline, now termed the Imaging and Medical Beamline (IMBL). The IMBL achieved 'first light' in December 2008 [1].
All research applications and scientific outcomes from this 3rd generation synchrotron beam are unique and the building of this facility has been achieved through the efforts of a wide range of scientists, technologists, engineers, mathematicians and, especially, materials scientists and physicists. Materials and condensed matter research is central to the development of specialised X-ray sources, sophisticated detectors and post-acquisition imaging capabilities. The biomedical applications and studies related here, whilst not exhaustive, highlight the rich collaborative framework that has developed at the Synchrotron and this brief overview provides an opportunity to relate some examples of biomedical science research that would not have been possible without access to this facility.

.

1. Introduction

The beamlines at the Australian Synchrotron provide substantial benefits to every area of science and technology in the nation. My personal view has always been that our knowledge and understanding of biology and human physiology have developed in parallel with our capacity to image cells and tissues as well as organs and body structures. These include advanced imaging modalities from microscopy for imaging of cells and tissues through to 2D and 3D macroscopic techniques for imaging of tissues and organs. Medical diagnoses, monitoring of disease progression, efficacy of therapies and the recent advent of 'targeted imaging' rely upon techniques such as X-ray analysis, Magnetic Resonance Imaging (MRI), Positron Emission Tomography (PET) and more. Access to high flux synchrotron X-radiation has now taken our medical research capabilities to a

new and internationally competitive level. Since the discovery of X-rays and development of medical X-ray sources, X-ray imaging has accounted for approximately 60% of medical diagnostic procedures; X-ray imaging is still the predominant technology used in medicine. The advent of high flux beams from synchrotron sources has revolutionized X-ray imaging and the capabilities can be seen by accessing any synchrotron facility website (www.synchrotron.org.au) (see Web link#1 in references). The high flux of the beam and broad selection of energies and bandwidths enables diverse applications in the field. This, aligned with sophisticated detector development, facilitates rapid data acquisition and high resolution imaging. This review focuses on the substantial benefits of access to synchrotron radiation in our research efforts in the biomedical sciences and biomedical imaging.

1.1 Background

This overview relates some of the background research and projects and publications from key groups associated with the AS. The reader should refer to several manuscripts for background theoretical aspects of X-ray science and advanced X-ray imaging, particularly phase-contrast X-ray imaging (PCXI) [2-6] and X-ray Fluorescence Microscopy (XFM) [7-9]. Many theoretical papers have been generated that describe aspects of phase-contrast X-ray imaging, X-ray computed tomography and development of X-ray sources, high resolution detectors and post-acquisition analysis. Substantial preliminary work on component development and detector design and production for the AS has been reported through the X-Ray Physics and Instrumentation Laboratory, CSIRO, headed for many years by the late Professor Steve Wilkins. Prof Wilkins was a pioneer in X-ray physics in Australia, a key player at the Australian National Beamline Facility (Photon Factory, Japan) and a key proponent for establishing the Australian Synchrotron.

1.2 Early projects conducted during design and building of the AS

1.2.1 PCXI of mouse tibia

In an early manuscript describing PCXI the authors related that PCXI would emerge as key technology to image at high resolution the progression of bone destruction in tumour metastases as well as other biological questions relating to diseases of the bone' [10]. Images depicted in Figure 1 show laboratory-based PCXI which provided information needed for the design of the PCXI systems on the IMBL. Development of X-TRACT™ software for post-acquisition X-ray tomography and analysis was also key to a successful outcome for the IMBL.

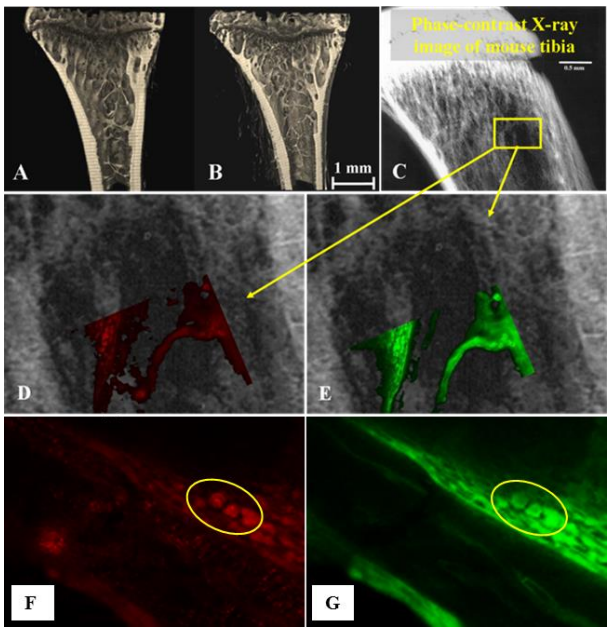

Fig. 1. 2D and 3D microsource PCXI of whole mouse tibiae and immuno- and cytochemical staining to identify osteoclasts**.** Panel A shows a control tibia and Panel B is a tibia exhibiting effects of a drug causing bone loss. These are whole bones imaged using PCI tomography (not rendered) and analysed with XTRACT™ for electronic sectioning. Microstructural changes, thinning of trabeculae and cortical bone and pitting of the endosteal surface could each be quantified. Panel C shows a transmission phase-contrast X-ray image acquired using a Fuji Film phosphorimager plate (original image 8,000 x 10,000 pixels), acquired for focusing and alignment, from which quantifiable digital data was obtained. Single cells can be identified in magnified images (theoretical effective resolution 4 microns). Panels D and E depict confocal LASER scanning microscope (CLSM) images superimposed over sample C to reveal osteoclasts on the trabecular network (CTR+ve by immunochemistry) and F-actin expressed at resorption front (Phalloidin Texas Red-X). Panels F and G highlight individual osteoclasts shown in D and E. The white scale-bar at top RHS is 0.5 mm.

1.2.2 Laboratory-based PCXI, the early research that aided sample preparation, detector development and post-acquisition analysis.

During the design phase of the beamlines, international synchrotrons have contributed substantially in terms of design, advice, loaned equipment and collaborative visits. The IMBL and the XFM beamlines have benefitted from substantial interactions with the European Synchrotron Research Facility (ESRF) Grenoble France, the Elettra Synchrotron (Sincrotone Trieste), and the National Synchrotron Light Source (New York; NSLS). The images shown in Figure 2 are samples imaged at the Elettra Sincrotrone for development of PCXI at the Australian Synchrotron; these were the same samples used for the first publication from the IMBL[1].

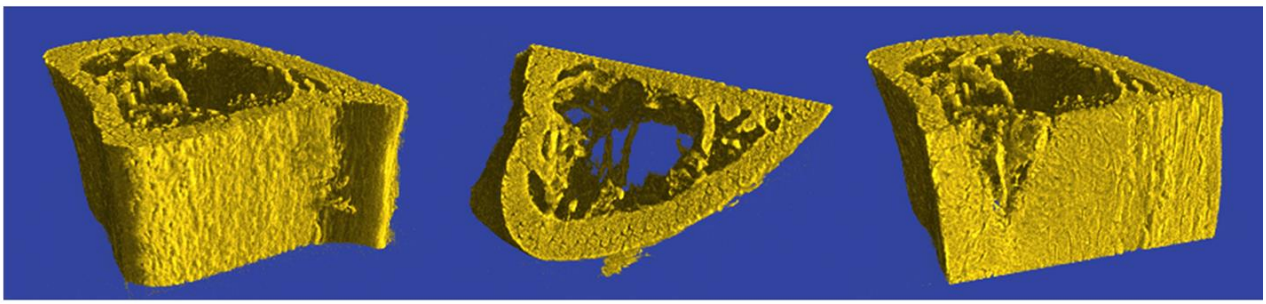

Fig. 2. Synchrotron CT of the same tibia samples at Elettra**.** These images show the surface rendered reconstructed CT images of section of tibia (diameter ~2.5 mm). These images depict the high resolution detail of trabecular structures and show features such as the Haversian and Volkmann channels. These samples were imaged and the tomography work and data processing done by Andrew Stevenson and Sherry Mayo (CSIRO, Australia) with Giuliana Tromba, Lucia Mancini and Luigi Rigon (Elettra Sincrotrone, Trieste, Italy).

2. The Australian Synchrotron Beamlines: Benefits to the biomedical sciences

2.1 The Imaging and Medical Beamline (IMBL)

As related above, the IMBL was the most complex of the beamlines to build and was therefore the last to be brought on-line to the scientific community. The IMBL was made possible through a special NHMRC grant submitted by the Planning Committee.

2.1.1 First images from the AS IMBL

Aspects relating to the design of the IMBL have been published [1, 11] and reconstructed images of the first sample, a mouse tibia from a study of a trophic endocrine regulator of bone turnover [12], are available through Web link#2 cited in the reference section.

2.1.2 Imaging bone sarcoma using PCXI on the IMBL

In a study on osteosarcoma invasion of bone, a sarcoma cell line was injected into the tibia of mice. An extensive imaging study was performed to assess two types of PET imaging (using [^{18}F]-FDG and [^{18}F]-Fluorine radioprobes) as reported [13]. IMBL images were analysed using Drishti software (see Web link#3) from IMBL PCXI data .These bone tumours, monitored over 12 weeks, are depicted in Figure 3 and show how tumours invaded the bone space causing extensive bone lysis.

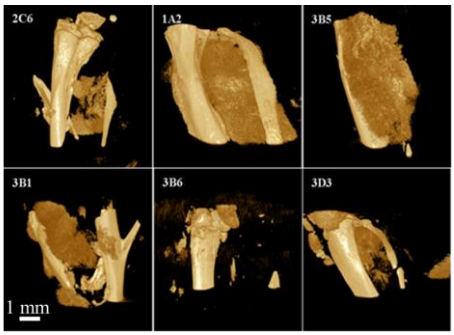

Fig. 3. Osteosarcoma in tibiae of mice imaged using phase-contrast X-ray imaging with synchrotron radiation on the IMBL at the Australian Synchrotron. Images of the osteosarcoma in bone depict the destruction of the bone and the substantial tumour infiltration. These images have been produced at 16 μm pixel resolution and reveal cell detail of bone, tumour and surrounding tissue. These images are actually 3D reconstructed images from hundreds of computed tomography slices and the bones can be sectioned electronically for quantification of tumour size, infiltration, volume of bone loss and bone lysis. Also, such 3D images can be co-registered with 3D PET images. This work was possible due to the generous support of the CASS Foundation (IM5234).

2.1.3 Dynamic imaging of lung function

Real-time synchrotron-based X-ray imaging of lung function has been achieved through projects conducted on BL20B2 bending magnet beamline at the SPring-8 synchrotron facility in Japan [14] and this and other structural/functional assessments of lung function [15, 16] are currently being implemented on the IMBL at the AS. These studies have investigated gene delivery systems as potential therapies for asthma and cystic fibrosis through to lung function studies investigating properties of surfactants during the initial air intake in neonates using small animal models.

2.1.4 Development of Microbeam Radiation Therapy (MRT) at the Australian Synchrotron

The IMBL has implemented X-ray microbeam radiotherapy (MRT), work developed in collaboration with synchrotron scientists from the European Synchrotron Radiation Facility (ESRF) in France [17-19]. Studies to evaluate dose-equivalents between MRT and broad beam X-radiation have been conducted [20-22] and work is on-going on small animal models [21, 23, 24]. MRT is generated by passing the synchrotron beam through a metal lattice that effectively breaks the beam into microbeams that are separated by 100-300 μm distance (about the width of a human hair). The width of each small beam can also be controlled, typically to 10-50 μm (see Web link#4 to MRT on the IMBL in reference section). Work to date has shown that the beam radiation doses are in the vicinity of 500-1000 Gy and that the effective radiation energy in the valleys between the microbeams are around 5-20 Gy (see AS website). Guidance protocols have also been established [25] and innovative ways to investigate MRT impacts on cells have been developed, including molecular pathways using gene analysis protocols [26].

2.2 X-ray fluorescence microscopy (XFM)

2.2.1 Adaption of XFM for biological samples.

XFM has been utilized extensively for materials and minerals research. The spectroscopy analysis program, GeoPIXE (PIXE is Proton-Induced X-ray Emission), was designed and adapted for the XFM beamline and then specifically tailored for data acquisition from the Maia _X-ray fluorescence detectors through a major collaboration between the CSIRO, the Australian Synchrotron and the Brookhaven laboratories at the National Synchrotron Light Source (NSLS) in the USA. The adaption of XFM to biological samples has proven very successful as the trace metal components in biological samples can depict the anatomical and cellular components within the biological samples [27-29]. This advance in technology has occurred due to development of the 'Maia Detector', an innovation led by the CSIRO [30-32]. XFM mapping of zinc in these brain samples reveals the synaptic connections of the neuronal networks. This is depicted in Figure 4 in which the pseudocoloured image shows Fe, Cu and Zn within the tissue. The samples prepared from the animals used in the VNI-funded TBI study were scanned using high definition mapping of trace metals on the XFM beam line at the AS using the MAIA-96 detector.

High-definition mapping of these elements, without any tissue histological staining or other technique, clearly resolves and defines the anatomical components of the tissue. The high quality and high resolution of the acquired spectral data enables quantification of trace metals down to the 'parts per million' (ppm) range. The scanning capabilities of the XFM endstation have been designed so that large sample areas can be imaged. Further work has been published describing the benefits of XFM in determining the detailed spatial organization of trace elements in brain slices with high sensitivity and high spatial resolution [33]. This paper described a sophisticated quantitative approach for analysis of trace metals using multi-element foils (MEF).

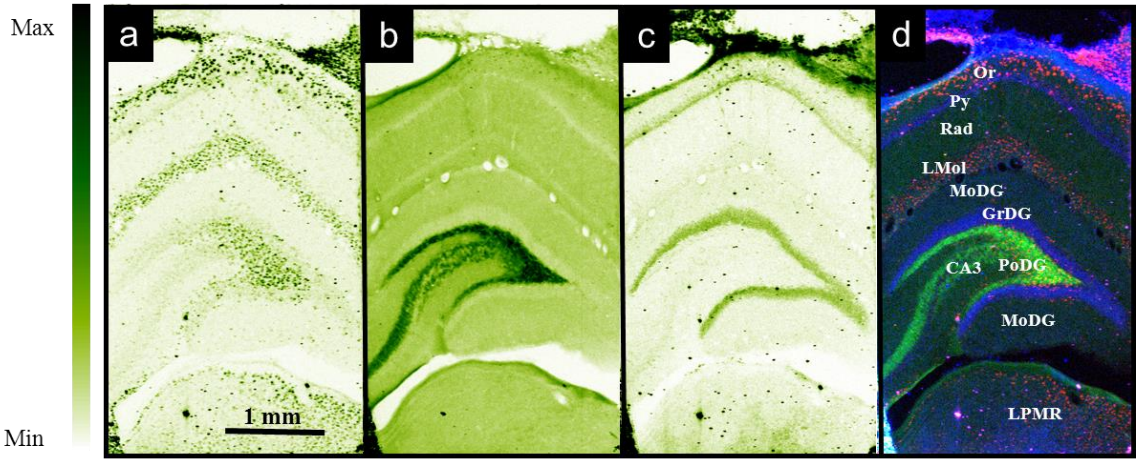

Fig. 4. Synchrotron-based XFM mapping of trace metal distribution within the hippocampus. Quantitative Fe, Cu and Zn maps in a brain slice from a rat; were acquired using Maia fly-scan acquisition on the XFM beamline. The maps of these trace metals clearly depict the lamellar structures of the hippocampus and the key structural components that define the hippocampal regions and the trisynaptic pathway: (a) Cu (with reference to Fig. 2 for the Nissl staining) associated with cell bodies of the hilar neurons and, above that, the *striatum* and cortex, respectively; (b) Zn is associated with neurons in the *hilus* and in the outer molecular layer and granular layer of the CA3 region; and, (c) Fe is most highly concentrated in the *dentate gyrus*). The colour-coded scale (LHS) depicts the concentration of each metal species in the sample with the maximum values for: Fe 101 ppm; Cu 28.9 ppm; Zn 69.6. The pseudo-colored image on the right (d) is a combined RGB image; Cu (red) and Zn (green) and Fe (blue), to demonstrate the spatial association of trace metals and the delineation of tissue structures. The regions are: Or, *Oriens* layer of HC; Py, Pyramidal cells; Rad, *radiatum* layer; LMol, *lacunosum moleculare*; GrDG, granular cells of *dentate gyrus*; CA3, *cornu ammonis* region 3; PoDG, polymorph region of the *dentate gyrus*; LPMR, lateral posterior thalamic nucleus, medial rostral part.

2.2.2 Imaging of brain slices in a model of closed-head traumatic brain injury (TBI)

Recently, we performed a major study on a small animal model of traumatic brain injury (TBI). This work was funded through the Victorian State Government Transport Accident Commission under a scheme called the Victorian Neurotrauma Initiative (VNI). Our group studied the complex neuronal changes and the structural, functional and affective changes that occurred as a consequence of TBI. As an extension of that study we decided to take some brain slice samples to the synchrotron. Research into TBI has relied upon advanced imaging modalities such MRI and FDG-PET but these techniques do not disclose changes at the neuronal network level. Images related in Figure 4 show how X-ray fluorescence spectroscopy of cryostat brain sections can show high resolution detail of the brain structures [34, 35]. Trace metal analysis was performed as previously described [33]. X-ray fluorescence microscopy (XFM) in this study has revealed features of the lamellar structures of the brain as an adjunct to histology and staining of neurons in thin slices of fixed brain tissues. These *in vivo* imaging studies included combined FDG-PET/MRI co-registration volumetric analysis [34, 35]. Cognitive, behavioural and epileptic outcomes were also studied and these data are available in the literature [36]. Extensive histology and post-mortem analysis also revealed underlying cellular and neuronal network changes caused by the head trauma and large-deformation high-dimensional mapping (LD-HDM) [37] highlighted the surface changes

that occurred to the hippocampus post-TBI. Cryostat sections of the brains from these same animals were mounted on 2 micron thick silicon nitride windows for imaging on the XFM beam line. Trace metal analysis was performed as previously described [33].

2.2.3 Preparation of brain slices from a well-characterised model of closed-head TBI for XFM

Images from our brain slice study of TBI samples (small animal model of closed-head injury) are depicted in Figure 4. These images are presented here to show the high resolution and accurate mapping of trace metals in these samples. This technique can provide unique information that is conveyed by both the images and the quantitative data. The definitive lamellar structures of the hippocampus are highlighted and the fine detail of the hippocampal structures and the zinc map alone reveals the neuronal networks within the hippocampus. This quantitative data relates the high definition mapping and spectral analysis for trace metals in the control group (the 'sham operated group' that did not receive a head trauma). These images and data are from cryostat sections from four (4) different animals in the study (Figure 4).

2.2.4 Summary of XFM technique applied to study of neuronal tissue

These images and data from this study highlight the adaptability of XFM for analysis of brain tissue slices, prepared during normal histological sectioning using cryostat cutting. This procedure could also be used for conventional wax-embedded microtome sections but with some minor adaptions as per James *et al.* [33]. XFM data has indicated that trace metals in specific regions of the hippocampus may be altered in the TBI group at 6 weeks post-trauma. Data suggests an elevation of zinc in the hilus in the TBI group and altered Fe levels in the dentate gyrus (preliminary data, unpublished). Each of Zn, Fe and Cu were distributed in specific layers or regions of the hippocampus. Analysis of four control tissues has established baseline levels of trace metals in regions of the hippocampus. Key findings included: (i) Zn, present in post-synaptic vesicles, was expressed in the hilus extending from the dentate gyrus to the CA3, tracking the mossy fibres of the trisynaptic pathway; (ii) The levels of zinc in the hilar region of the CA3, were at high levels (28.9±1.3 ppm) compared to the molecular layer of the dentate gyrus (9.8±1.6 ppm) and in the CA3 region where a high level of mossy fibre synaptic connections are present (22.4±0.8 ppm); (iii) Fe was associated with distinct lamellae of the hippocampus in the molecular layer where the cell bodies of the neurons (axons) are present; (iv) The distribution of Fe was high in the molecular layer of the dentate gyrus (20.4±3.1 ppm) and at moderate levels in the hilus (8.1±3.3 ppm) and CA3 regions (9.4±3.8 ppm); and, (v) Cu could be discerned at the cellular level in discrete foci associated with hilar neurons (15.5±3.5 ppm as depicted in the ROI) but, in comparison, levels of Fe were very low in the DG (6.2±1.2 ppm) and in the CA3 region (6.4±1.7 ppm). These data have highlighted the potential of XFM for spatial high definition mapping of trace metal elements in brain and other tissues. The capacity to map metal elements at the cellular level within the broad context of the entire sample has provided a powerful tool to investigate normal tissues and pathology of neurodegenerative conditions and disease processes.

2.3 X-Ray Crystallography (MX1 and MX2)

The first of the macro-molecular crystallography beamlines to become operational was MX1, an X-ray crystallaography beamline, designed for chemical and biological structure analysis. MX1 incorporates a bending magnet with a very stable beam and can analyse single crystals whilst the neighbouring MX2 beamline incorporates a finer focus using 'in-vacuum' undulator source and microcollimator. MX2 facilitates samples that are difficult to crystallise and/or weakly-diffracting samples such as viruses, nucleic acids and other organic molecules. A broad range of manuscripts have been published from the MX1/MX2 beamlines predominantly related to determination of molecular structures of growth factors, transmembrane proteins and enzyme-ligand interactions [38-40].

2.4 X-ray absorption spectroscopy (XAS)

Determining the biological properties of metals has been elusive but high flux synchrotron beams may now enable determination of the structure/function relationships in metalloproteins [41]. An example of the key role of metals in disease processes and proposed therapies is the role of selenium as a supplement in some forms of cancer. Determination of selenium bio-distribution and speciation in tumour cells may provide information relevant for tumour therapies [42].

2.5 Soft X-ray

This beamline has been designed for surface science studies and investigation of the materials physics of samples exhibiting appropriate emission properties. Whilst this beamline is principally used to investigate solid state inorganic materials, it is also able to measure certain biologically-based materials and substrates relevant to membrane properties and drug development. An example of work has been the determination of chiral orientation of metal substrates used in drug design and manufacture [43] and plasma polymer interface interactions have been studied for biological compounds on solid surfaces relevant to drug manufacture [44].

2.6 SAXS/WAXS

Small- and wide-angle X-ray scattering enables the characterisation of biologically relevant macromolecules such as proteins. Samples for SAXS do not need to be in crystalline form and instead can be in a more amenable form such as colloids, suspensions, gels and so forth. Examples of applications beneficial to the biological sciences is fatty acid analysis of nanoparticles proposed for delivery of drugs and assessment/analysis of contrast agents for medical imaging [45]. An example of interpretative capability is the study of the hydration state of a long-used antiepileptic drug, carbamazepine, relevant to understanding drug solubility and absorption in the gut. Work on this beamline has included the study of substrate specificity of bacterial enzymes [46] as well as photoactivated release of compounds from lipid-based matrix to improve drug delivery [47].

2.7 Powder Diffraction

The Powder Diffraction beamline has been designed for materials science application and the study of microporous structures. Applications are predominantly related to understanding mineral structure such as in the soil sciences and in engineering applications but the beamline has been used to study pharmaceutical materials with regards to solubility and phase transitions in biological environments as well as structural analysis of proteins in lipid membranes [48, 49].

2.8 FTIRM and THz/Far-IR

Application of focal plane array-Fourier transform infrared (FPA-FTIR) microspectroscopy has been applied to the analysis of matrix in MSC chondrogenesis experiments [50] and determination of whether PTH affects bone matrix mineral composition [51]. The THz/Far-IR beamline enables spectroscopic analysis of gases and molecules with low absorption coefficients. This beamline has also been used for study of thin films and materials applications. Examples cited on the AS website include the study of pigments and protein structures. However, the Far-IR beamline is not particularly suited to complex or large biological samples.

3. Discussion

The Australian Synchrotron now provides access to a 3rd generation high flux beam with unique characteristics that can be modulated through to multiple beamlines. The examples presented here highlight the adaptability, diversity and potential range of techniques that can now be implemented into our projects. As each of the beamlines are improved and developed further biomedical applications will become available. An extensive list of all publications can be obtained from the Australian Synchrotron website. The Australian Synchrotron provides an important tool for our scientific communities across the entire Australasian-Pacific region. The AS beam lines, nine at present, have diverse applications that can be accessed by all academic disciplines. The examples related here were included to highlight the biomedical applications and advanced imaging

that has been possible and these capabilities will now expand. The same determination and passion that carried the argument for the building of this facility are now being directed to the importance of the recurrent funding as well as the new 'innovation funds' that are critically needed to keep Australia at the forefront of medical research. To date, the Australian Synchrotron has fulfilled the high expectations set during the planning, development and building phases of the project. Further, the Australian Synchrotron has delivered exemplary scientific outcomes that are evidence of the success of a multidisciplinary as well national and international collaborative approach.

4. Conclusion

The purpose of this brief overview was to highlight some features of the Australian Synchrotron, show some data sets and images that demonstrate how the beamlines have added substantially to current projects and, also, to spark the imaginations of our younger scientists who should consider the diverse applications available at the Australian Synchrotron that will, for decades to come, add value to our research efforts in many fields including physics, materials science, biomedical science, the arts and more.

Acknowledgments

Work on the beamlines at the Australian Synchrotron has been funded through diverse granting bodies, universities, institutes and through state governments and, particularly, the Federal Government. Specific work cited herein related to work on the IMBL was funded through a special grant from the NHMRC. Also, some of the minor projects were funded through a University of Melbourne Research Grant Support Scheme (CIs DE Myers and AW Stevenson); Work on the bone samples and the MRT was funded through the Australian Orthopaedics Association (DE Myers P Choong and MT Broadhead) and through the CASS Foundation (CIA Myers); The TBI work was funded through the Victorian Neurotrauma Initiative by the Transport Accident Commission (CIs TJ O'Brien, DE Myers and RJ Hicks) and other contributors to this work included Prof Vivienne Bouilleret, Ms Lisa Carbone, Mr John Williams, Dr Nigel Jones and several students who worked on that project at the time.

References

1. Stevenson, A.W., et al., *First experiments on the Australian Synchrotron Imaging and Medical beamline, including investigations of the effective source size in respect of X-ray imaging.* J Synchrotron Radiat, 2010. **17**(1): p. 75-80.
2. Gureyev, T.E., et al., *Refracting Röntgen's rays: Propagation-based x-ray phase contrast for biomedical imaging* Journal of Applied Physics, 2009. **105**: p. 102005.
3. Gureyev, T.E., et al., *Some simple rules for contrast, signal-to-noise and resolution in in-line x-ray phase-contrast imaging.* Opt Express, 2008. **16**(5): p. 3223-41.
4. Gureyev, T.E., et al., *Quantitative methods in phase-contrast x-ray imaging.* J Digit Imaging, 2000. **13**(2 Suppl 1): p. 121-6.
5. Nesterets, Y., et al., *Soft tissue small avascular tumor imaging with x-ray phase-contrast micro-CT in-line holography.* Proc SPIE Int Soc Opt Eng, 2008. **6913**: p. 69133z.
6. Paganin, D., et al., *Simultaneous phase and amplitude extraction from a single defocused image of a homogeneous object.* J Microsc, 2002. **206**(Pt 1): p. 33-40.
7. Fahrni, C.J., *Biological applications of X-ray fluorescence microscopy: exploring the subcellular topography and speciation of transition metals.* Curr Opin Chem Biol, 2007. **11**(2): p. 121-7.
8. Paunesku, T., et al., *X-ray fluorescence microprobe imaging in biology and medicine.* J Cell Biochem, 2006. **99**(6): p. 1489-502.
9. Jones, K.W., et al., *X-ray fluorescence with synchrotron radiation.* Ultramicroscopy, 1988. **24**(2-3): p. 313-28.
10. Wilkins, S.W., et al., *Phase-contrast imaging using polychromatic hard X-rays.* Nature, 1996. **384**(6607): p. 335.

11. Stevenson, A.W., et al., *Analysis and interpretation of the first monochromatic X-ray tomography data collected at the Australian Synchrotron Imaging and Medical beamline.* J Synchrotron Radiat, 2012. **19**(Pt 5): p. 728-50.
12. Cornish, J., et al., *Leptin directly regulates bone cell function in vitro and reduces bone fragility in vivo.* J Endocrinol, 2002. **175**(2): p. 405-15.
13. Broadhead, M.L., et al., *Applying Advanced Imaging Techniques to a Murine Model of Orthotopic Osteosarcoma.* Front Surg, 2015. **2**: p. 36.
14. Dubsky, S., et al., *Synchrotron-based dynamic computed tomography of tissue motion for regional lung function measurement.* J R Soc Interface, 2012. **9**(74): p. 2213-24.
15. Parsons, D.W., et al., *High-resolution visualization of airspace structures in intact mice via synchrotron phase-contrast X-ray imaging (PCXI).* J Anat, 2008. **213**(2): p. 217-27.
16. Siu, K.K., et al., *Phase contrast X-ray imaging for the non-invasive detection of airway surfaces and lumen characteristics in mouse models of airway disease.* Eur J Radiol, 2008. **68**(3 Suppl): p. S22-6.
17. Renier, M., et al., *The radiotherapy clinical trials projects at the ESRF: technical aspects.* Eur J Radiol, 2008. **68**(3 Suppl): p. S147-50.
18. Serduc, R., et al., *Characterization and quantification of cerebral edema induced by synchrotron x-ray microbeam radiation therapy.* Phys Med Biol, 2008. **53**(5): p. 1153-66.
19. Siegbahn, E.A., et al., *Determination of dosimetrical quantities used in microbeam radiation therapy (MRT) with Monte Carlo simulations.* Med Phys, 2006. **33**(9): p. 3248-59.
20. Crosbie, J.C., et al., *Reference dosimetry at the Australian Synchrotron's imaging and medical beamline using free-air ionization chamber measurements and theoretical predictions of air kerma rate and half value layer.* Med Phys, 2013. **40**(6): p. 062103.
21. Ibahim, M.J., et al., *An evaluation of dose equivalence between synchrotron microbeam radiation therapy and conventional broad beam radiation using clonogenic and cell impedance assays.* PLoS One, 2014. **9**(6): p. e100547.
22. Priyadarshika, R.C., et al., *Biodosimetric quantification of short-term synchrotron microbeam versus broad-beam radiation damage to mouse skin using a dermatopathological scoring system.* Br J Radiol, 2011. **84**(1005): p. 833-42.
23. Crosbie, J.C., et al., *Tumor cell response to synchrotron microbeam radiation therapy differs markedly from cells in normal tissues.* Int J Radiat Oncol Biol Phys, 2010. **77**(3): p. 886-94.
24. Yang, Y., et al., *In vitro study of genes and molecular pathways differentially regulated by synchrotron microbeam radiotherapy.* Radiat Res, 2014. **182**(6): p. 626-39.
25. Pelliccia, D., et al., *Image guidance protocol for synchrotron microbeam radiation therapy.* J Synchrotron Radiat, 2016. **23**(2): p. 566-73.
26. Sprung, C.N., et al., *Genome-wide transcription responses to synchrotron microbeam radiotherapy.* Radiat Res, 2012. **178**(4): p. 249-59.
27. House, M.J., et al., *Mapping iron in human heart tissue with synchrotron x-ray fluorescence microscopy and cardiovascular magnetic resonance.* J Cardiovasc Magn Reson, 2014. **16**: p. 80.
28. Wang, P., et al., *Quantitative determination of metal and metalloid spatial distribution in hydrated and fresh roots of cowpea using synchrotron-based X-ray fluorescence microscopy.* Sci Total Environ, 2013. **463-464**: p. 131-9.
29. Lye, J.C., et al., *Detection of genetically altered copper levels in Drosophila tissues by synchrotron x-ray fluorescence microscopy.* PLoS One, 2011. **6**(10): p. e26867.
30. Ryan, C., *PIXE and the nuclear microprobe: Tools for quantitative imaging of complex natural materials.* Nuclear Instruments and Methods in Physics Research: Section B Beam Interactions with Materials and Atoms., 2011. **269**(20): p. 2151-2162.
31. Pascolo, L., et al., *Synchrotron X-ray microscopy reveals early calcium and iron interaction with crocidolite fibers in the lung of exposed mice.* Toxicol Lett, 2016. **241**: p. 111-20.

32. Lombi, E., et al., *Trends in hard X-ray fluorescence mapping: environmental applications in the age of fast detectors.* Anal Bioanal Chem, 2011. **400**(6): p. 1637-44.
33. James, S.A., et al., *Quantitative comparison of preparation methodologies for X-ray fluorescence microscopy of brain tissue.* Anal Bioanal Chem, 2011. **401**(3): p. 853-64.
34. Liu, Y.R., et al., *Progressive metabolic and structural cerebral perturbations after traumatic brain injury: an in vivo imaging study in the rat.* J Nucl Med, 2010. **51**(11): p. 1788-95.
35. Bouilleret, V., et al., *Progressive brain changes on serial manganese-enhanced MRI following traumatic brain injury in the rat.* J Neurotrauma, 2009. **26**(11): p. 1999-2013.
36. Jones, N.C., et al., *Experimental traumatic brain injury induces a pervasive hyperanxious phenotype in rats.* J Neurotrauma, 2008. **25**(11): p. 1367-74.
37. Hogan, R.E., et al., *MRI-based large deformation high dimensional mapping of the hippocampus in rats: development and validation of the technique.* J Magn Reson Imaging, 2009. **29**(5): p. 1027-34.
38. Dogovski, C., et al., *From knock-out phenotype to three-dimensional structure of a promising antibiotic target from Streptococcus pneumoniae.* PLoS One, 2013. **8**(12): p. e83419.
39. Gunn, N.J., et al., *Purification, crystallization, small-angle X-ray scattering and preliminary X-ray diffraction analysis of the SH2 domain of the Csk-homologous kinase.* Acta Crystallogr Sect F Struct Biol Cryst Commun, 2011. **67**(Pt 3): p. 336-9.
40. Soares da Costa, T.P., et al., *Structural Determinants Defining the Allosteric Inhibition of an Essential Antibiotic Target.* Structure, 2016. **24**(8): p. 1282-91.
41. George, G.N., et al., *X-ray-induced photo-chemistry and X-ray absorption spectroscopy of biological samples*. Journal of Synchrotron Radiation, 2012. **19**: p. 875-886.
42. Weekley, C.M., et al., *Selenium metabolism in cancer cells: the combined application of XAS and XFM techniques to the problem of selenium speciation in biological systems.* Nutrients, 2013. **5**(5): p. 1734-56.
43. Tadich, A., et al., *Determining the Orientation of a Chiral Substrate Using Full-Hemisphere Angle-Resolved Photoelectron Spectroscopy*. Physical Review Letters, 2011. **PRL 107**: p. 175501.
44. Chen, R.T., et al., *New Insights into the Substrate Plasma Polymer Interface.* J. Phys. Chem. B, 2011. **115**: p. 6495–6502.
45. Tran, N., et al., *High-Throughput Screening of Saturated Fatty Acid Influence on Nanostructure of Lyotropic Liquid Crystalline Lipid Nanoparticles.* Langmuir, 2016. **32**(18): p. 4509-20.
46. Khandokar, Y.B., et al., *Structural and Functional Characterization of the PaaI Thioesterase from Streptococcus pneumoniae Reveals a Dual Specificity for Phenylacetyl-CoA and Medium-chain Fatty Acyl-CoAs and a Novel CoA-induced Fit Mechanism.* J Biol Chem, 2016. **291**(4): p. 1866-76.
47. Fong, W.K., et al., *External manipulation of nanostructure in photoresponsive lipid depot matrix to control and predict drug release in vivo.* J Control Release, 2016. **228**: p. 67-73.
48. Dilanian, R.A., et al., *A new approach for structure analysis of two-dimensional membrane protein crystals using X-ray powder diffraction data.* Protein Sci, 2011. **20**(2): p. 457-64.
49. Khan, J., et al., *In Situ Lipolysis and Synchrotron Small-Angle X-ray Scattering for the Direct Determination of the Precipitation and Solid-State Form of a Poorly Water-Soluble Drug During Digestion of a Lipid-Based Formulation.* J Pharm Sci, 2016. **105**(9): p. 2631-9.

50. Chonanant, C., et al., *Discrimination of micromass-induced chondrocytes from human mesenchymal stem cells by focal plane array-Fourier transform infrared microspectroscopy.* Talanta, 2014. **130**: p. 39-48.
51. Vrahnas, C., et al., *Anabolic action of parathyroid hormone (PTH) does not compromise bone matrix mineral composition or maturation.* Bone, 2016. **93**: p. 146-154.

Web link#1 to the Australian Synchrotron: www.synchrotron.org.au

Web link#2 to 'First images from the IMBL':
https://www.youtube.com/watch?v=vnBTsVlQLAY&list=PLziMe3ErTg5PalzX7I2kaCrYCF1bvdAMe&index=15

Web link#3 to Drishi reference and access: http://anusf.anu.edu.au/Vizlab/drishti/

Web link#4 to MRT on the IMBL:
http://www.synchrotron.org.au/aussyncbeamlines/imaging-medical/higlights-im/microbeam-radiotherapy-experiments-at-imbl).